AD-A218 823

DTIC FILE COPY

TECHNICAL REPORT BRL-TR-3073

BRL

A MODIFIED LAGRANGE PRESSURE GRADIENT FOR THE REGENERATIVE LIQUID PROPELLANT GUN

WALTER F. MORRISON
TERENCE P. COFFEE

JANUARY 1990

APPROVED FOR PUBLIC RELEASE; DISTRIBUTION UNLIMITED.

U.S. ARMY LABORATORY COMMAND

BALLISTIC RESEARCH LABORATORY
ABERDEEN PROVING GROUND, MARYLAND

DESTRUCTION NOTICE

Destroy this report when it is no longer needed. DO NOT return it to the originator.

Additional copies of this report may be obtained from the National Technical Information Service, U.S. Department of Commerce, Springfield, VA 22161.

The findings of this report are not to be construed as an official Department of the Army position, unless so designated by other authorized documents.

The use of trade names or manufacturers' names in this report does not constitute indorsement of any commercial product.

UNCLASSIFIED

SECURITY CLASSIFICATION OF THIS PAGE

REPORT DOCUMENTATION PAGE

Form Approved
OMB No. 0704-0188

1a. REPORT SECURITY CLASSIFICATION: Unclassified	1b. RESTRICTIVE MARKINGS
2a. SECURITY CLASSIFICATION AUTHORITY	3. DISTRIBUTION / AVAILABILITY OF REPORT: Approved for public release; distribution unlimited
2b. DECLASSIFICATION / DOWNGRADING SCHEDULE	
4. PERFORMING ORGANIZATION REPORT NUMBER(S): BRL-TR-3073	5. MONITORING ORGANIZATION REPORT NUMBER(S)
6a. NAME OF PERFORMING ORGANIZATION: US Army Ballistic Research Laboratory; 6b. OFFICE SYMBOL (If applicable): SLCBR-IB	7a. NAME OF MONITORING ORGANIZATION
6c. ADDRESS (City, State, and ZIP Code): Aberdeen Proving Ground, MD 21005-5066	7b. ADDRESS (City, State, and ZIP Code)
8a. NAME OF FUNDING / SPONSORING ORGANIZATION; 8b. OFFICE SYMBOL (If applicable)	9. PROCUREMENT INSTRUMENT IDENTIFICATION NUMBER
8c. ADDRESS (City, State, and ZIP Code)	10. SOURCE OF FUNDING NUMBERS: PROGRAM ELEMENT NO. / PROJECT NO. / TASK NO. / WORK UNIT ACCESSION NO

11. TITLE (Include Security Classification)
A MODIFIED LAGRANGE PRESSURE GRADIENT FOR THE REGENERATIVE LIQUID PROPELLANT GUN

12. PERSONAL AUTHOR(S)
Morrison, Walter F. and Coffee, Terence P.

13a. TYPE OF REPORT	13b. TIME COVERED	14. DATE OF REPORT (Year, Month, Day)	15. PAGE COUNT
TR	FROM _____ TO _____		

16. SUPPLEMENTARY NOTATION

17. COSATI CODES			18. SUBJECT TERMS (Continue on reverse if necessary and identify by block number)
FIELD	GROUP	SUB-GROUP	

19. ABSTRACT (Continue on reverse if necessary and identify by block number)

A modified Lagrange gradient model for use in lumped parameter simulations of the regenerative liquid propellant gun is presented. The model accounts for the non-zero gas velocity at the barrel entrance and the rarefaction wave traveling along the barrel toward the projectile base after all-burnt in a regenerative liquid propellant gun (RLPG). Computer simulations of a high velocity cannon have been conducted utilizing a lumped parameter code with the modified Lagrange gradient and a second lumped parameter code with a one-dimensional barrel flow model. Comparisons of muzzle velocities, pressure versus time curves, and velocity and pressure profiles in the barrel are presented. The modified Lagrange gradient model provides results which are nearly indistinguishable from those obtained using the one- dimensional model over the entire ballistic cycle. Calculated muzzle velocities agree to within 1-3% over the range 1500-2000 m/s, with the best agreement at the lower velocities.

20. DISTRIBUTION / AVAILABILITY OF ABSTRACT	21. ABSTRACT SECURITY CLASSIFICATION	
☐ UNCLASSIFIED/UNLIMITED ☒ SAME AS RPT. ☐ DTIC USERS	Unclassified	
22a. NAME OF RESPONSIBLE INDIVIDUAL: Walter F. Morrison	22b. TELEPHONE (Include Area Code): (301) 278-6189	22c. OFFICE SYMBOL: SLCBR-IB-B

DD Form 1473, JUN 86 *Previous editions are obsolete.* SECURITY CLASSIFICATION OF THIS PAGE

INTENTIONALLY LEFT BLANK.

TABLE OF CONTENTS

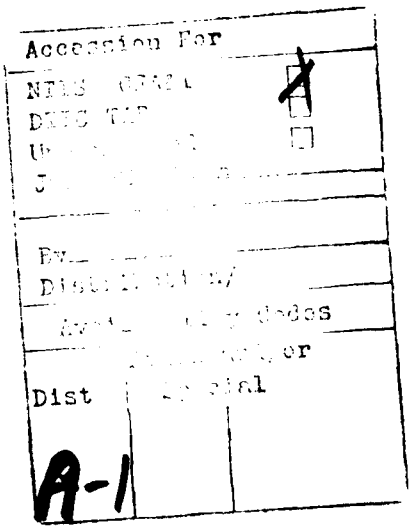

INTENTIONALLY LEFT BLANK.

LIST OF FIGURES

LIST OF FIGURES (CON'T)

I. INTRODUCTION

Over the past several years, a number of computer models of the regenerative interior ballistic process have been developed. The two models which have been used most frequently at the Ballistic Research Laboratory are the models developed by Coffee[1] and Gough.[2] The Coffee model utilizes lumped parameter descriptions for the three main regions in the regenerative gun: the propellant reservoir, the combustion chamber and the barrel. In contrast, Gough has chosen to treat the reservoir and chamber as lumped parameter regions, while utilizing a one-dimensional flow model for the barrel region.

In order to model the barrel as a lumped parameter region, a pressure gradient model, analogous to the standard Lagrange gradient used in many solid propellant gun models,[3] is required. The pressure gradient model simulates the drop in pressure from the breech or barrel entrance to the projectile base, which results from the velocity gradient developed as the projectile accelerates down the barrel. The development of such a pressure gradient model requires that the unique features of the regenerative interior ballistic (IB) process be incorporated into the model. The pertinent features are the non-zero gas velocity at the entrance to the barrel and the existence of a rarefaction wave traveling along the barrel toward the projectile base after all-burnt.

In the following paper, the development of a modified Lagrange gradient model, which accounts for the unique features of the regenerative IB process, is described. The modified Lagrange gradient has been incorporated into the lumped parameter interior ballistic model developed by Coffee,[1] and computer simulations of a hypothetical 120-mm tank cannon have been conducted. Simulations were also conducted using the Coffee[1] model with a standard Lagrange gradient and the Gough[2] model with a one-dimensional barrel flow model. Using the results from the Gough model as a baseline, comparisons of muzzle velocities, pressure versus time curves, and detailed velocity and pressure profiles in the barrel are presented and discussed.

II. THE LAGRANGE PRESSURE GRADIENT

The equations of motion governing the motion of the gas in a gun in the region from breech to projectile base are

$$\frac{\partial \rho}{\partial t} + v\frac{\partial \rho}{\partial x} + \rho\frac{\partial v}{\partial x} = 0, \tag{1}$$

$$\rho\left[\frac{\partial v}{\partial t} + v\frac{\partial v}{\partial x}\right] = -\frac{\partial P}{\partial x}, \tag{2}$$

with the boundary conditions

$$x_{BREECH} = 0, \tag{3}$$

$$x_{BASE} = y, \tag{4}$$

$$v_{BREECH} \triangleq v_L = 0, \tag{5}$$

$$v_{BASE} \triangleq v_R = \frac{dy}{dt} = u_p, \tag{6}$$

where u_p is the velocity of the projectile.

In the development of the Lagrange pressure gradient "it is assumed all the propellant charge, C, is in gaseous form at the time considered". However, "the theory applies without alteration if it is assumed that", prior to consumption of all the propellant charge, "the unburnt charge moves with the gas, the distribution of the solid along the bore being the same as the distribution of gas."[3]

We now assume that the density of the gas (or gas plus unburnt charge) is uniform over the region behind the projectile,

$$\frac{\partial \rho}{\partial x} = 0 \quad . \tag{7}$$

We then obtain from Equation (1)

$$\frac{\partial \rho}{\partial t} + \rho \frac{\partial v}{\partial x} = 0$$

or

$$\frac{\partial v}{\partial x} = -\frac{1}{\rho}\frac{\partial \rho}{\partial t} \quad . \tag{8}$$

Assuming a constant bore area, A_B, (i.e., no chambrage) and noting that $\rho = C/A_b y$. Equation (8) becomes

$$\frac{\partial v}{\partial x} = \frac{1}{y}\frac{\partial y}{\partial t} = \frac{u_p}{y} \quad . \tag{9}$$

Integrating (9) over the region [0,y], we obtain

$$v(x) = \left(\frac{x}{y}\right) u_p \quad . \tag{10}$$

Corner notes that the term "Lagrange approximation" is applied to Equation (7) or (10) and that Equation (7) leads to Equation (10), but it is not true that Equation (10) necessarily implies Equation (7).[3]

Substituting Equation (10) in Equation (2), we have

$$\left(\frac{x}{y}\right) u_p = -\frac{1}{\rho}\frac{\partial P}{\partial x}$$

or

$$\frac{\partial P}{\partial x} = -\frac{C u_p}{A_B}\left(\frac{x}{y^2}\right) \quad . \tag{11}$$

Integrating on [0,y], and noting that

$$\ddot{u}_p = \frac{(P_{BASE} - P_{RES})A_B}{M_p},$$

$$P(0) = P_{BREECH} \ ,$$

and

$$P(y) = P_{BASE} \ ,$$

where P_{RES} is the bore resistance pressure and M_p is the projectile mass, we obtain

$$P(x) = P_{BASE} + \frac{C}{2M_p}(P_{BASE} - P_{RES})\left(1 - \frac{x^2}{y^2}\right) \ . \tag{12}$$

For x = 0,

$$P_{BREECH} = P_{BASE} + \frac{C}{2M_p}(P_{BASE} - P_{RES}) \ . \tag{13}$$

The space mean pressure is defined by

$$\bar{P} = \frac{1}{y}\int_0^y P(x)dx, \tag{14}$$

and upon substituting Equation (12), we obtain

$$\bar{P} = P_{BASE} + \frac{C}{3M_p}(P_{BASE} - P_{RES}) \ . \tag{15}$$

The kinetic energy associated with the motion of the gas is

$$KE_{GAS} = \int_0^y \frac{1}{2} A_B \rho v^2 dx. \tag{16}$$

Using Equation (10) we obtain

$$KE_{CAS} = \frac{1}{2} A_s \rho \frac{u_p^2}{y^2} \left[\frac{1}{3} x^3 \right]_0^y$$

or

$$KE_{CAS} = \frac{1}{6} C u_p^2 \quad . \tag{17}$$

The solution after "all-burnt" (to muzzle exit) is based on the assumption that the gases expand adiabatically such that

$$\left[P_{BREECH} \left(\frac{1}{\rho} - n \right)^\gamma \right]_{ALL\text{-}BURNT} = \text{CONSTANT} \quad .$$

However, this portion of the solution is not pertinent to the model developed in subsequent sections, and will not be discussed here.

III. DESCRIPTION OF THE RLPG INTERIOR BALLISTIC PROCESS

The RLPG IB process is based on the injection of the propellant into the combustion chamber during the IB cycle. The stages of the IB process are depicted in Figure 1 for the RLPG configuration known as Concept VI.

The system consists of 3 regions: (1) The liquid reservoir bounded by the regenerative piston, the fixed bolt, and the transducer block; (2) the combustion chamber; and (3) the barrel. In regenerative gun concepts similar to Concept VI, there is a large area change (about a factor of 4) from the combustion chamber into the barrel.

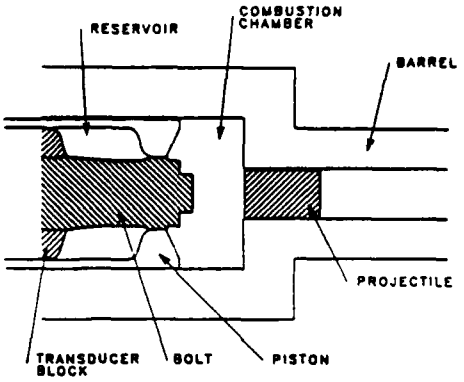

1A

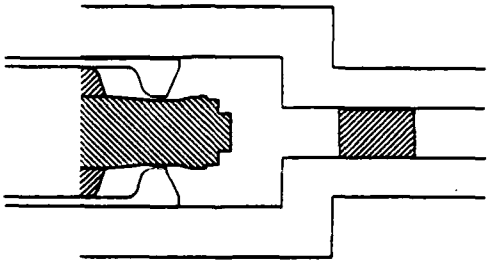

1B

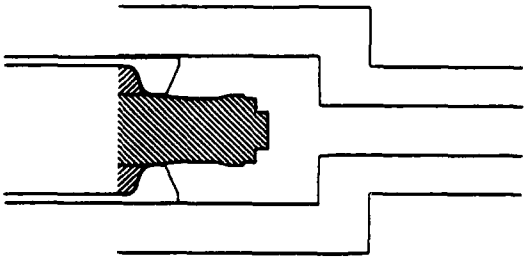

1C

Figure 1. Regenerative Liquid Propellant Gun, Concept VI

Initially, the piston is seated on the front of the bolt, sealing the propellant in the reservoir; see Figure 1(a). The process is initiated by firing an igniter into the combustion chamber, which generates an initial pressure in the chamber; see Figure 2.

The increasing chamber pressure acts on the regenerative piston, forcing it to the rear, thus pressurizing the propellant reservoir. Due to the area difference across the piston face from the chamber to the reservoir, the piston acts as a pump, resulting in (1) a pressure in the liquid reservoir which is higher than that in the combustion chamber, and (2) injection of propellant into the combustion chamber.

As the piston moves to the rear over the contoured, fixed bolt, the injection area first increases to a maximum value associated with the maximum design pressure of the system and then decreases, decelerating the piston as it completes its stroke; see Figure 1(b). When shot-start pressure is exceeded, the projectile begins accelerating down the tube. Analyses[4] of experimental data indicate that early in the ballistic cycle, significant amounts of unburnt propellant may accumulate in the combustion chamber, that this accumulated propellant is rapidly consumed as the pressure rises to its maximum value, and that propellant subsequently injected is rapidly consumed leading to very low values of propellant accumulation in the latter stages of the ballistic cycle; see Figure 2. Such analyses would also indicate that over <u>most</u> of the projectile travel, propellant is consumed rapidly in the combustion chamber with little accumulation, and, therefore, only small amounts of unburnt propellant would be transferred into the barrel.

Utilizing such analyses, most regenerative IB models have been based on the following assumptions:

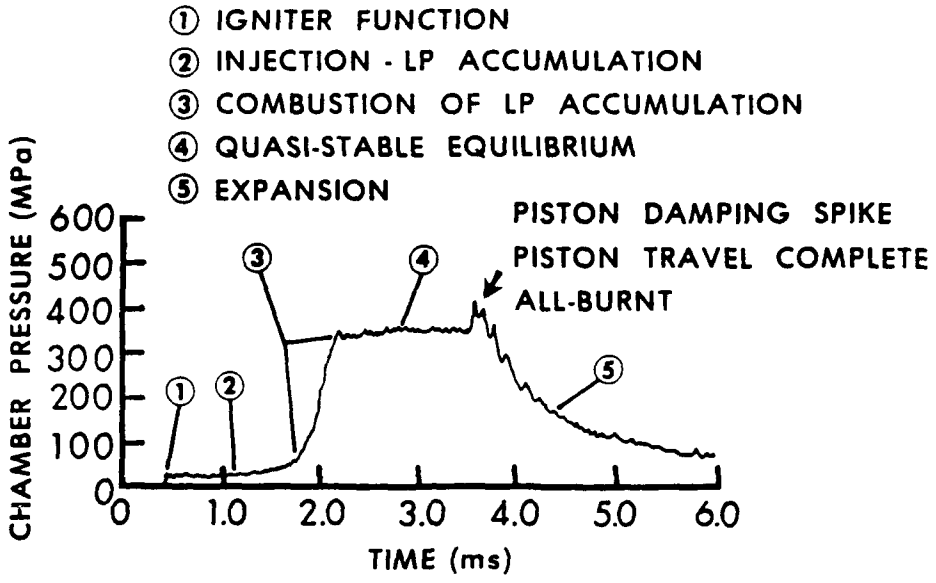

Figure 2. A Pressure Versus Time Curve From an Early Simple In-Line Piston RLPG Concept, Annotated to Show the Phases of the Regenerative Interior Ballistic Process.

1. The combustion chamber is a homogeneous region containing either a two-phase mixture of propellant droplets and combustion gases (if a finite rate droplet burning model is used), or combustion gases only (if an instantaneous propellant burning model is assumed).

2. Only combustion gases enter the barrel region.

3. As the gases enter the barrel, they undergo an expansion process.

The lumped parameter model developed by Coffee does permit a two-phase mixture and droplet combustion in the barrel region, i.e., assumption 2 is relaxed, but this option has not been exercised extensively. The fully one-dimensional IB model recently developed by Gough[5] treats the combustion chamber as a non-homogeneous region and also permits a two-phase mixture and

droplet combustion in the barrel region. Investigations using this model of the effects of relaxing assumptions 1 and 2 are underway, but results are not yet available.

Following the completion of piston motion, the remaining propellant in the combustion chamber (and barrel) is quickly consumed, leading to the "all-burnt" condition. Prior to all-burnt, the gases required to maintain the operating pressure, under the conditions of rapid expansion resulting from piston motion in the chamber and projectile motion in the barrel, are supplied by propellant combustion, primarily in the chamber region. Upon burnout, the combustion chamber pressure rapidly decreases and a rarefaction wave would be expected to move along the barrel toward the projectile base.

This phenomena was originally suggested by Morrison et al,[6] based on simulations using the one-dimensional model developed by Gough;[2] see Figure 3. (It appears similar to the phenomena reported in solid propellant systems utilizing stick propellant charges by Robbins and Horst.[7]) Recent analyses of data from 25-mm regenerative test firings conducted in the mid-1970's provide experimental verification of the existence of such a rarefaction wave;[8] see Figure 4. In these tests, pressure gages were located at several points along the barrel. The resulting pressure profiles are non-monotonic along the barrel, with the point of maximum pressure moving toward the base of the projectile, indicating the presence of a rarefaction wave.

The ballistic process is completed with muzzle exit and "blow-down" of the gases remaining in the barrel.

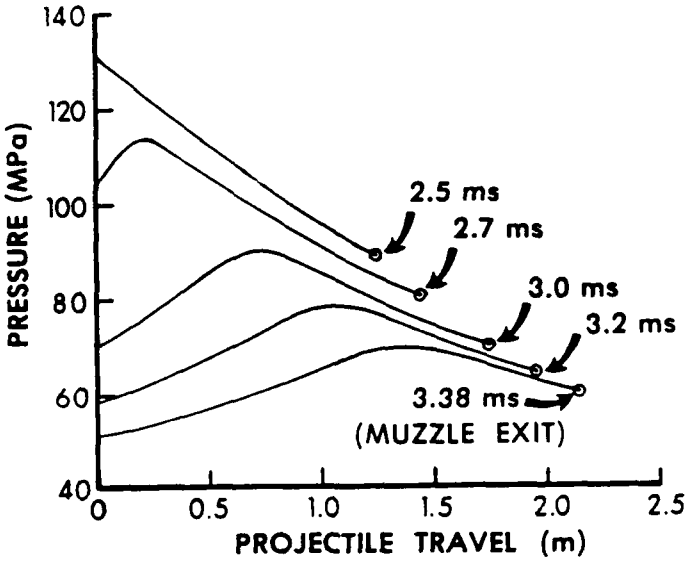

Figure 3. Pressure Profiles in the Barrel at Various Times During the Ballistic Cycle, Taken From A One-Dimensional Simulation[6] of a 25-mm RLPG.

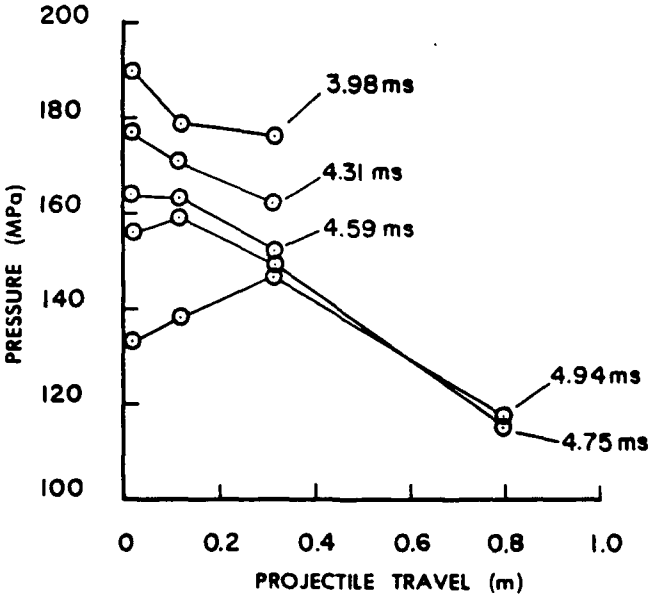

Figure 4. Experimental Pressure Profiles[7] in the Barrel of a 25-mm RLPG (GE Shot No. 41) at Various Times in the Ballistic Cycle after P_{Max} Showing the Development of a Rarefaction Wave in the Barrel after All-Burnt.

IV. MODIFIED LAGRANGE PRESSURE GRADIENT

From the preceding discussion, it is obvious that the standard Lagrange pressure gradient does not accurately reflect the physical process in the barrel region of a regenerative gun. The shortcomings of the standard Lagrange model are as follows:

1. The expansion of the combustion gases from the chamber into the barrel with a large area reduction is not treated.

2. The non-zero gas velocity at the entrance to the tube and the time dependence of the mass of combustion gases in the barrel are not accounted for.

3. The rarefaction wave in the barrel after all-burnt is not simulated.

In order to simulate these processes in the interior ballistics model, modifications to the standard Lagrange pressure gradient model are required. In the following development, it is assumed for simplicity that only combustion gases enter the barrel. However, the development applies equally to a two-phase mixture of combustion gases and propellant droplets if the assumption of uniform mixture density is made.

1. EXPANSION OF COMBUSTION GASES FROM THE COMBUSTION CHAMBER INTO THE BARREL

The barrel region is treated as a single control volume into which combustion gases flow from the chamber. The left-hand boundary of the control volume is defined by the barrel entrance, while the right boundary is defined by the base of the projectile. The subscript c denotes combustion chamber conditions, L denotes the left boundary conditions and R denotes the right boundary conditions. Therefore,

$$x_{ENTRANCE} \triangleq x_L = 0, \tag{18}$$

$$x_{BASE} \triangleq x_R = y, \tag{19}$$

and so on.

In a steady state, isentropic flow system, $h+v^2/2$ is a conserved quantity, where h is the enthalpy. Therefore,

$$h_c + \frac{1}{2}v_c^2 = h_L + \frac{1}{2}v_L^2 + \frac{1}{2}\left[\left(\frac{1}{\psi}\right) - 1\right]^2 v_L^2, \tag{20}$$

where the last term on the right-hand-side has been introduced to account for the head loss in the flow as the gases enter the barrel. We note that

$$h = c_p T + \eta P \tag{21}$$

for a gas obeying the Nobel-Abel equation-of-state and assume that the expansion of the combustion gases into the tube is isentropic, i.e.,

$$P_c^{1/\gamma}\left(\frac{1}{\rho_c} - \eta\right) = P_L^{1/\gamma}\left(\frac{1}{\rho_L} - \eta\right). \tag{22}$$

Using Equations (21) and (22) in Equation (20), we obtain, after some algebraic manipulation,

$$\frac{P_L}{P_c} = \left\{ 1 + \frac{2\eta(P_c - P_L) - \left[v_L^2 \left(1 + \left[\left(\frac{1}{\psi} \right) - 1 \right]^2 \right) - v_c^2 \right]}{2 c_p T_c} \right\}^{\frac{\gamma}{\gamma - 1}} \quad . \tag{23}$$

It is assumed that $v_c = 0$ in Equation (23), which then defines the pressure drop from the chamber to the barrel. This equation is used in both the Coffee[1,9] and Gough[2] models to connect the chamber and barrel regions.

2. MODIFIED LAGRANGE PRESSURE GRADIENT; BEFORE ALL-BURNT

We must now solve the equations of motion for the gases in the barrel, Equations (1) and (2), with the boundary conditions

$$x_L = 0, \tag{24}$$

$$x_R = y, \tag{25}$$

$$v_L \neq 0, \tag{26}$$

$$v_R = u_p, \tag{27}$$

and with the Lagrange assumption, Equation (7). From the continuity equation, we obtain

$$\frac{\partial v}{\partial x} = -\frac{1}{\rho}\frac{\partial \rho}{\partial t}. \tag{8}$$

Noting that the mass of combustion gases in the barrel, m, is a function of time and that $\rho = m/A_B x_R$, we obtain

$$\frac{\partial \rho}{\partial t} = \frac{\dot{m}}{A_B x_R} - \frac{m u_p}{A_B x_R^2},$$

such that

$$\frac{\partial v}{\partial x} = -\frac{1}{\rho}\frac{\partial \rho}{\partial t} = -\frac{\dot{m}}{m} + \frac{u_p}{x_R}, \tag{28}$$

where the time rate of change of the mass of the gases in the barrel, $\dot{m}$, is $\rho A_B v_L$. Therefore,

$$\frac{\partial v}{\partial x} = \frac{u_p}{x_R} - \frac{v_L}{x_R}. \tag{29}$$

Integrating on [0,x], we have

$$v(x) = u_p\left(\frac{x}{x_R}\right) + v_L\left(1 - \frac{x}{x_R}\right), \tag{30}$$

and

$$\dot{v}(x) = \dot{u}_p\left(\frac{x}{x_R}\right) + \dot{v}_L\left(1 - \frac{x}{x_R}\right) - u_p(u_p - v_L)\left(\frac{x}{x_R^2}\right) \quad . \tag{31}$$

Substituting Equation (30) and (31) in Equation (2), and noting that

$$\dot{u}_p = (P_{BASE} - P_{RES})\frac{A_B}{M_p},$$

we obtain

$$-\frac{1}{\rho}\frac{\partial P}{\partial x} = \{\dot{v}_L\left(1 - \frac{x}{x_R}\right) + \frac{A_B}{M_p}(P_{BASE} - P_{RES})\left(\frac{x}{x_R}\right) - u_p(u_p - v_L)\left(\frac{x}{x_R^2}\right) + \left[v_L + (u_p - v_L)\left(\frac{x}{x_R}\right)\right]\frac{u_p - v_L}{x_R}\} \quad . \tag{32}$$

Integrating on [0,x], we have

$$P(x) = P_L - \rho\{\frac{A_B}{2M_p}(P_{BASE} - P_{RES})\frac{x^2}{x_R} + \left[\dot{v}_L + \frac{1}{x_R}v_L(u_p - v_L)\right]\left[x - \frac{1}{2}\frac{x^2}{x_R}\right]\} \quad . \tag{33}$$

Note that Equations (30) and (33) reduce to (10) and (12) if $v_L = \dot{v}_L = 0$ and $m = C$.

Using the definition of the space mean pressure, Equation (14), we now integrate Equation (33) on $[0, x_R]$ to obtain

$$\bar{P} = P_L - \frac{m}{6M_p}(P_{BASE} - P_{RES}) - \frac{m}{3A_B}\left[\dot{v}_L + \frac{v_L(u_p - v_L)}{x_R}\right]. \tag{34}$$

Similarly, using the definition for the kinetic energy of the gas, Equation (16), and substituting from Equation (30), we have

$$KE_{GAS} = \frac{m}{6}(u_p^2 + u_p v_L + v_L^2). \tag{35}$$

3. MODIFIED LAGRANGE PRESSURE GRADIENT; AFTER ALL-BURNT

In the description of the RLPG interior ballistic process, we discussed the rarefaction wave which travels along the barrel from the chamber toward the projectile base after propellant burnout. We model the rarefaction wave as a discontinuity in the spatial derivatives of velocity and pressure, which travels along the barrel at a velocity equal to the average speed of sound in the gas plus the local gas velocity; see Figure 5. Since this discontinuity resembles a "hinge" in the velocity and pressure distributions, we have labeled it the "hinge point" and quantities at the hinge point are denoted by the subscript H. This representation of a contact discontinuity in a gun tube was recently suggested by Gough.[10] The velocity of the hinge point, x_H, is then

$$\frac{\partial x_H}{\partial t} = v_H + a. \tag{36}$$

The hinge point divides the barrel into two regions:

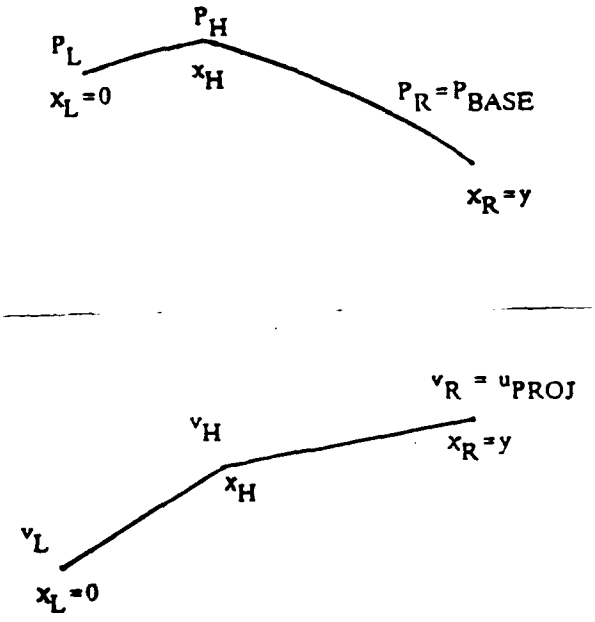

Figure 5. Schematic Showing the Hinge-Points in the Bilinear Velocity Distribution and Pressure Distribution, Which is Quadratic on Either Side of the Hinge-Point.

Region I: $0 \leq x \leq x_H$

and

Region II: $x_H < x \leq x_R$.

a. Solution in Region I: We assume that the velocity distribution is linear in both regions I and II, i.e. we use the second form of the "Lagrange Approximation" noted by Corner[3]. From Figure 5, we see that

$$\frac{\partial v_I(x)}{\partial x} = \frac{v_H - v_L}{x_H}, \qquad 0 \le x < x_H, \tag{37}$$

and integrating on [0, x_H] we obtain

$$v_I(x) = v_H\left(\frac{x}{x_H}\right) + v_L\left(1 - \frac{x}{x_H}\right). \tag{38}$$

Using (38) in Equation (2), we have

$$-\frac{1}{\rho}\frac{\partial P_I}{\partial x} = \left[\dot{v}_H - \frac{a(v_H - v_L)}{x_H}\right]\left(\frac{x}{x_H}\right) + \left[\dot{v}_L + \frac{v_L(v_H - v_L)}{x_H}\right]\left(1 - \frac{x}{x_H}\right). \tag{39}$$

We have assumed that mass entering the barrel after all-burnt is distributed uniformly over the barrel region, such that there is a uniform gas density in the barrel, consistent with the basic Lagrange assumption. Integrating (39) on [0,x] gives us the pressure distribution in Region I,

$$P_I(x) = P_L - \rho\left\{\left[\dot{v}_H - \frac{a(v_H - v_L)}{x_H}\right]\left(\frac{x^2}{2x_H}\right) + \left[\dot{v}_L + \frac{v_L(v_H - v_L)}{x_H}\right]\left(x - \frac{x^2}{2x_H}\right)\right\}, \tag{40}$$

where

$$v_H = \frac{\partial}{\partial t}\left\{v_{II}(x)\Big|_{x_H}\right\}. \tag{41}$$

b. Solution in Region II: It is assumed that at burnout $x_H = x_L = 0$ and that the hinge point, x_B, then propagates down the barrel toward the projectile base at a velocity given by Equation (36). Since x_B propagates at the speed of sound plus the local gas velocity, Region II is acoustically isolated from events in the combustion chamber. Therefore, we assume that the linear velocity gradient in Region II is determined by the value of v_L at the time of burnout, v_{Lb}, such that

$$\frac{\partial v_{II}(x)}{\partial x} = \frac{v_R - v_{Lb}}{x_R}, \qquad x_{,1} \le x \le x_R. \tag{42}$$

Then

$$v_{II}(x) = v_R\left(\frac{x}{x_R}\right) + v_{Lb}\left(1 - \frac{x}{x_R}\right), \tag{43}$$

$$v_H = v_R\left(\frac{x_H}{x_R}\right) + v_{Lb}\left(1 - \frac{x_H}{x_R}\right), \tag{44}$$

and

$$\dot{v}_H = \left(\frac{v_R - v_{Lb}}{x_R}\right)(v_H + \alpha) + \dot{v}_R\frac{x_H}{x_R} - v_R(v_R - v_{Lb})\frac{x_H}{x_R^2}. \tag{45}$$

We now use (43) in Equation (2) to obtain

$$-\frac{1}{\rho}\frac{\partial P_{II}}{\partial x} = v_r\left(\frac{x}{x_R}\right) + \left[v_{Lb} + \frac{v_{Lb}(v_R - v_{Lb})}{x_R}\right]\left(1 - \frac{x}{x_R}\right), \tag{46}$$

and integrating on $[x_H, x]$, we have

$$P_{II}(x) = P_H - \rho\{\dot{v}_R\left(\frac{x^2 - x_H^2}{2x_R}\right) + \left[\dot{v}_{Lb} + \frac{v_{Lb}(v_R - v_{Lb})}{x_R}\right]\left[(x - x_H) - \frac{x^2 - x_H^2}{2x_R}\right]\}, \quad (47)$$

where,

$$v_R = u_p, \quad (48)$$

$$\dot{v}_R = \dot{u}_p = \frac{(P_{BASE} - P_{RES})A_B}{M_p}, \quad (49)$$

and from (40), we have

$$P_H = P_L - \rho\left\{(\dot{v}_L + \dot{v}_H)\frac{x_H}{2} + \frac{1}{2}(v_H - v_L)(v_L - a)\right\}. \quad (50)$$

c. Space Mean Pressure; After All-Burnt: We again use the definition of Space Mean Pressure, Equation (14),

$$\bar{P} = \frac{1}{x_R}\int_0^{x_R} P(x)dx = \frac{1}{x_R}\left\{\int_0^{x_H} P_I(x)dx + \int_{x_H}^{x_R} P_{II}(x)dx\right\}. \quad (51)$$

Defining $\bar{P}_I$ and $\bar{P}_{II}$,

$$\bar{P}_I = \frac{1}{x_R}\int_0^{x_H} P_I(x)dx, \tag{52}$$

$$\bar{P}_{II} = \frac{1}{x_R}\int_{x_H}^{x_R} P_{II}(x)dx, \tag{53}$$

we have

$$\bar{P}_I = P_L\left(\frac{x_H}{x_R}\right) - \frac{\rho x_H^2}{x_R}\left\{\frac{1}{6}\left[\dot{v}_H - \frac{a(v_H - v_L)}{x_H}\right] + \frac{1}{3}\left[\dot{v}_L + \frac{v_L(v_H - v_L)}{x_H}\right]\right\}, \tag{54}$$

and

$$\bar{P}_{II} = P_H\left(\frac{x_R - x_H}{x_R}\right) - \frac{\rho}{6x_R^2}\{\dot{v}_R(x_R - x_H)^2(x_R + 2x_H) + 2\left[\dot{v}_{Lb} + \frac{v_{Lb}(v_R - v_{Lb})}{x_R}\right](x_R - x_H)^3\}. \tag{55}$$

Combining (54) and (55) and using Equation (50), we have for the space mean pressure

$$\bar{P} = P_L - \frac{\rho x_H}{2}\left\{\left[\dot{v}_H - \frac{a(v_H - v_L)}{x_H}\right]\left(1 - \frac{2x_H}{3x_R}\right) + \left[\dot{v}_L + \frac{v_L(v_H - v_L)}{x_H}\right]\left(1 - \frac{x_H}{3x_R}\right)\right\} - \frac{\rho x_R}{6}\{\dot{v}_R\left[\left(1 - \frac{x_H}{x_R}\right)^2\left(1 + \frac{2x_H}{x_R}\right)\right] + 2\left[\dot{v}_{Lb} + \frac{v_{Lb}(v_R - v_{Lb})}{x_R}\right]\left(1 - \frac{x_H}{x_R}\right)^3\}. \tag{56}$$

d. Kinetic Energy of the Gas in the Barrel: After All-Burnt: The Kinetic Energy of the gas is given by Equation (16),

$$KE_{GAS} = \int_0^{x_R} \frac{1}{2} A_B \rho v^2 dx.$$

Substituting from (38) and (43), we have

$$KE_{GAS} = \frac{1}{2} A_B \rho \left\{ \int_0^{x_H} v_I^2(x) dx + \int_{x_H}^{x_R} v_{II}^2(x) dx \right\}. \tag{57}$$

Defining KE_I and KE_{II}, we have

$$KE_I = \frac{\rho A_B x_H}{6} (v_H^2 + v_H v_L + v_L^2), \tag{58}$$

$$KE_{II} = \frac{\rho A_B x_R}{6} \{ v_R^2 \left[1 - \left(\frac{x_H}{x_R} \right)^3 \right] + v_R v_{Lb} \left[1 - 3 \left(\frac{x_H}{x_R} \right)^2 \left(1 - \frac{2x_H}{3x_R} \right) \right] + v_{Lb}^2 \left(1 - \frac{x_H}{x_R} \right)^3 \}. \tag{59}$$

and finally,

$$KE_{GAS} = \frac{m}{6} \{ [v_H^2 + v_H v_L + v_L^2] \left(\frac{x_H}{x_R} \right) + v_R^2 \left[1 - \left(\frac{x_H}{x_R} \right)^3 \right] + v_R v_{Lb} \left[1 - 3 \left(\frac{x_H}{x_R} \right)^2 \left(1 - \frac{2x_H}{3x_R} \right) \right] + v_{Lb}^2 \left(1 - \frac{x_H}{x_R} \right)^3 \}. \tag{60}$$

V. INTERIOR BALLISTICS MODEL

The modified Lagrange gradient has been implemented in the lumped parameter model developed by Coffee.[9] This model includes descriptions of the propellant reservoir, piston motion, propellant injection, the combustion chamber including propellant combustion, mass transfer to the barrel region, gas flow in the barrel, and projectile motion. The changes required to implement the modified Lagrange gradient involved only the portions of the model dealing with mass transfer from the chamber to the barrel and gas flow in the barrel.

1. STANDARD LAGRANGE GRADIENT MODEL

In the original version of the Coffee model,[9] a standard Lagrange gradient is used, and the gas velocity at the entrance to the barrel is ignored. The space mean pressure is calculated from the lumped parameter energy equation for the barrel. P_{BASE} is determined from equation (15), substituting the instantaneous mass of the gas in the barrel, m, for the charge, C,

$$P_{BASE} = \left[\bar{P} + \frac{m}{3M_p} P_{RES}\right] / \left[1 + \frac{m}{3M_p}\right] . \tag{61}$$

Similarly, P_L (which is equivalent to P_{BREECH} in this case) is obtained from Equation (13),

$$P_L = P_{BASE} + \frac{m}{2M_p}(P_{BASE} - P_{RES}). \tag{62}$$

The mass flux into the barrel is

$$\dot{m} = \rho_L A_B v_L . \tag{63}$$

where v_L is obtained from Equation (23) with $v_c = 0$.

$$v_L = \left\{ 2c_p T_c \left[1 - \left(\frac{P_L}{P_c} \right)^{\frac{\gamma-1}{\gamma}} \right] + 2n(P_c - P_L) \right\}^{\frac{1}{2}} . \tag{64}$$

(Since we have neglected head loss in performing the calculations discussed in subsequent sections, we have set $\psi = 1$ in writing Equation (64).) The gas density at the left boundary, ρ_L, is not equal to the mean gas density in the barrel, but is rather obtained from Equation (22). The kinetic energy of the gas in the barrel is given by Equation (17).

2. MODIFIED LAGRANGE GRADIENT MODEL

In the implementation of the modified Lagrange gradient, ordinary differential equations for $\dot{v}_L$ (i.e., the ODE's for $\dot{v}_L$ are different before and after all-burnt) must be introduced such that v_L is calculated directly in the solution of the coupled ODE model equations. The pressure at the left boundary, P_L, is obtained by iteratively solving the non-linear Equation (23) using the Newton-Raphson technique. As in the case of the standard Lagrange gradient model, the space mean pressure is calculated from the lumped parameter energy equation for the barrel and the mass flux into the barrel is defined by Equation (63).

a. <u>Model Equations Prior to All-Burnt:</u> Prior to all-burnt, the pressure at the projectile base, P_{BASE}, is determined using Equations (33) and (34). We first evaluate Equation (33) at x_R to obtain

$$P_{BASE} = P_L - \frac{m}{2M_p}(P_{BASE} - P_{RES}) - \frac{m}{2A_B}\left[\dot{v}_L + \frac{v_L(u_p - v_L)}{x_R} \right]. \tag{65}$$

Using Equation (65) in Equation (34) to eliminate the terms involving u_p, v_L and $\dot{v}_L$, we have

$$P_{BASE} = \left[\frac{3}{2}\bar{P} - \frac{1}{2}P_L + \frac{m}{4M_p}P_{RES}\right] \Big/ \left[1 + \frac{m}{4M_p}\right] . \tag{66}$$

Alternatively, we could have used Equation (65) in Equation (34) to eliminate P_L, obtaining

$$P_{BASE} = \left\langle \bar{P} + \frac{m}{3M_p}P_{RES} - \frac{m}{6A_B}\left[\dot{v}_L + \frac{v_L(u_p - v_L)}{x_R}\right]\right\rangle \Big/ \left[1 + \frac{m}{3M_p}\right] . \tag{67}$$

(which reduces to the standard Lagrange gradient, Equation (61), for $v_L = \dot{v}_L = 0$.) The required ordinary differential equation for $\dot{v}_L$ is then obtained by rewriting Equation (65), i.e.,

$$\dot{v}_L = \{\frac{2A_B}{m}\left[P_L - P_{BASE}\left(1 + \frac{m}{2M_p}\right) + P_{RES}\frac{m}{2M_p}\right] - \frac{v_L(u_p - v_L)}{x_R}\} . \tag{68}$$

The kinetic energy of the gas in the barrel is defined by Equation (35).

b. Model Equations After All-Burnt: Following the completion of propellant combustion, the pressure at the projectile base, P_{BASE}, is given by Equation (47) evaluated at x_R, i.e.,

$$P_{BASE} = P_L - \frac{\rho x_R}{2}\left(1 - \frac{x_H^2}{x_R^2}\right)\dot{u}_p - \frac{\rho x_H}{2}\dot{v}_L - T_1 , \tag{69}$$

where we have made use of Equations (48) and (50) and where

$$T_1 = \frac{\rho x_H}{2}\left[\dot{v}_H + \frac{(v_H - v_L)(v_L - a)}{x_H}\right] + \frac{\rho x_R}{2}\left[\dot{v}_{Lb} + \frac{v_{Lb}(u_p - v_{Lb})}{x_R}\right]\left(1 - \frac{x_H}{x_R}\right)^2. \tag{70}$$

Using Equation (56) to eliminate the term involving $\dot{v}_L$, we obtain, after some algebraic manipulation,

$$P_{BASE} = \left[\bar{P} + \frac{m}{3M_p}P_{RES}\left(1 - \frac{x_H}{2x_R} - \frac{x_H^3}{2x_R^3}\right) - \left(\frac{x_H}{3x_R}\right)P_L - \left(1 - \frac{x_H}{3x_R}\right)T_1 + T_2\right] / \left[\left(1 - \frac{x_H}{3x_R}\right) + \frac{m}{3M_p}\left(1 - \frac{x_H}{2x_R} - \frac{x_H^3}{2x_R^3}\right)\right], \tag{71}$$

where,

$$T_2 = \frac{\rho x_H}{2}\left\{\left[\dot{v}_H - \frac{a(v_H - v_L)}{x_H}\right]\left(1 - \frac{2x_H}{3x_R}\right) + \left[\frac{v_L(v_H - v_L)}{x_H}\right]\left(1 - \frac{x_H}{3x_R}\right)\right\} + \frac{\rho x_R}{3}\left[\dot{v}_{Lb} + \frac{v_{Lb}(u_p - v_{Lb})}{x_R}\right]\left(1 - \frac{x_H}{x_R}\right)^3. \tag{72}$$

(We note that for $v_{Lb} = \dot{v}_{Lb} = 0$ and $x_H = 0$ Equation (71) reduces to Equation (61), the standard Lagrange gradient.) The ordinary differential equation for $\dot{v}_L$ is then obtained by rewriting Equation (69), i.e.,

$$\dot{v}_L = \frac{2A_B}{m}\left(\frac{x_R}{x_H}\right)\left\{P_L - P_{BASE}\left[1 + \frac{m}{2M_p}\left(1 - \frac{x_H^2}{x_R^2}\right)\right] + P_{RES}\frac{m}{2M_p}\left(1 - \frac{x_H^2}{x_R^2}\right) - T_1\right\} \tag{73}$$

The kinetic energy of the gas in the barrel is defined by Equation (60).

The resulting sets of coupled ODE and algebraic equations are then solved using the implicit ODE solver, EPISODE.

VI. DESCRIPTION OF TEST CASE

In order to assess the modified Lagrange gradient model, a series of test cases was developed. Since the largest effect would be expected in high velocity, high charge-to-mass ratio situations, a hypothetical 120-mm regenerative LP tank cannon used in an earlier study[11] was selected. The charge mass and other gun parameters, with the exception of liquid injection area, were held constant. Three projectile masses were used to provide a range of velocities, and the liquid injection area was adjusted for each projectile mass to produce a maximum chamber pressure of 500 MPa. A hypothetical liquid gun propellant was also used in the simulation. This propellant has the thermochemistry of JA-2 and the physical properties of a HAN-based LP. This choice was made to provide somewhat higher projectile velocities than would be achievable with a HAN-based LP in the specific cannon configuration used in the study, in order to permit evaluation of the modified Lagrange gradient model under the most adverse conditions practical. The gun parameters and thermochemical data used in the simulations are provided in Tables 1 and 2.

TABLE 1. 120-mm Cannon Parameters

Caliber	120 mm
Propellant Mass	16.8 kg
Projectile Mass*	5 kg, 7 kg, 13 kg
Projectile Travel	6.3 m
Initial Chamber Volume	6000 cm^3
Reservoir Volume	11700 cm^3
Chamber Diameter	34.2 cm
Liquid Injection Area*	94 cm^2, 76 cm^2, 60 cm^2
Max Chamber Pressure	500 MPa
Max Reservoir Pressure	700 MPa

*Injection Area for 5 kg projectile is 94 cm^2, etc.

TABLE 2. Propellant Data

	Liquid JA-2	LGP 1846
Impetus	1140 J/g	898 J/g
Flame Temperature	3409 K	2468 K
Ratio of Specific Heats	1.225	1.223
Co-Volume	.996 cm^3/g	.677 cm^3/g
c_p	1.821 J/g-K	1.999 J/g-K
Density	1.43 g/cm^3	1.43 g/cm^3

VII. RESULTS

Computer simulations for the three test cases were made using the lumped parameter IB model developed by Coffee[9] with both the standard and modified Lagrange gradient models. Simulations were also run using an IB model developed by Gough.[2] The Gough model treats the reservoir and chamber as lumped parameter regions and utilizes Equation (23) to connect the chamber with the barrel, which is modeled as a one-dimensional flow region.

Since a one-dimensional model should provide a more accurate simulation of the barrel region, the Gough model was selected as a baseline for evaluation of the Lagrange gradient models.

Both models were run assuming instantaneous burning of propellant injected into the combustion chamber. As a result, the simulations of the reservoir and chamber regions are nearly identical in the Gough and Coffee models, and any differences in the overall model calculations are primarily due to differences in the simulation of the barrel region.

The calculated muzzle velocities for the nine cases simulated (3 projectile masses and 3 gradient models) are presented in Table 3.

TABLE 3. Comparison of Calculated Muzzle Velocities

Gough Model One-Dimensional Flow		Coffee Model Standard Lagrange Gradient		Coffee Model Modified Lagrange Gradient	
Projectile Mass (kg)	Muzzle Velocity (m/s)	Muzzle Velocity (m/s)	Difference (%)	Muzzle Velocity (m/s)	Difference (%)
5.0	2020	2121	5.0	1952	-3.4
7.0	1894	1983	4.7	1849	-2.3
13.0	1563	1622	3.8	1546	-1.1

The differences between the muzzle velocities calculated using the Lagrange gradients and those obtained from the Gough models are presented as a percent of the baseline velocity. As can be seen, use of the standard Lagrange gradient consistently results in muzzle velocities higher than the baseline case, while use of the modified Lagrange gradient results in velocities which are lower than the baseline. Overall, the velocities obtained using the modified Lagrange gradient are somewhat closer to the baseline than those obtained with the standard gradient, and the agreement degrades with increasing velocity.

The pressure versus time curves from the simulations with the 7 kg projectile mass are presented in Figures 6a and 6b. In Figure 6a, the pressure versus time curves at three locations (chamber, barrel entrance and projectile base) obtained using the Coffee model with the standard Lagrange gradient (dotted line) are presented along with the corresponding pressure curves obtained using the Gough model for comparison. A similar comparison is presented in Figure 6b for the modified Lagrange gradient.

As can be seen in Figure 6a, the chamber pressures are quite similar, but the pressure versus time curves at the barrel entrance and projectile base show significant differences. The standard Lagrange gradient results in a pressure at the projectile base which is consistently higher than that obtained with the one-dimensional model, resulting in a higher muzzle velocity; see Table 3. The pressure at the barrel entrance for the standard Lagrange gradient case is

consistently lower than that for the one-dimensional case. Overall, the standard Lagrange gradient model produces results quite different from the baseline, one-dimensional model.

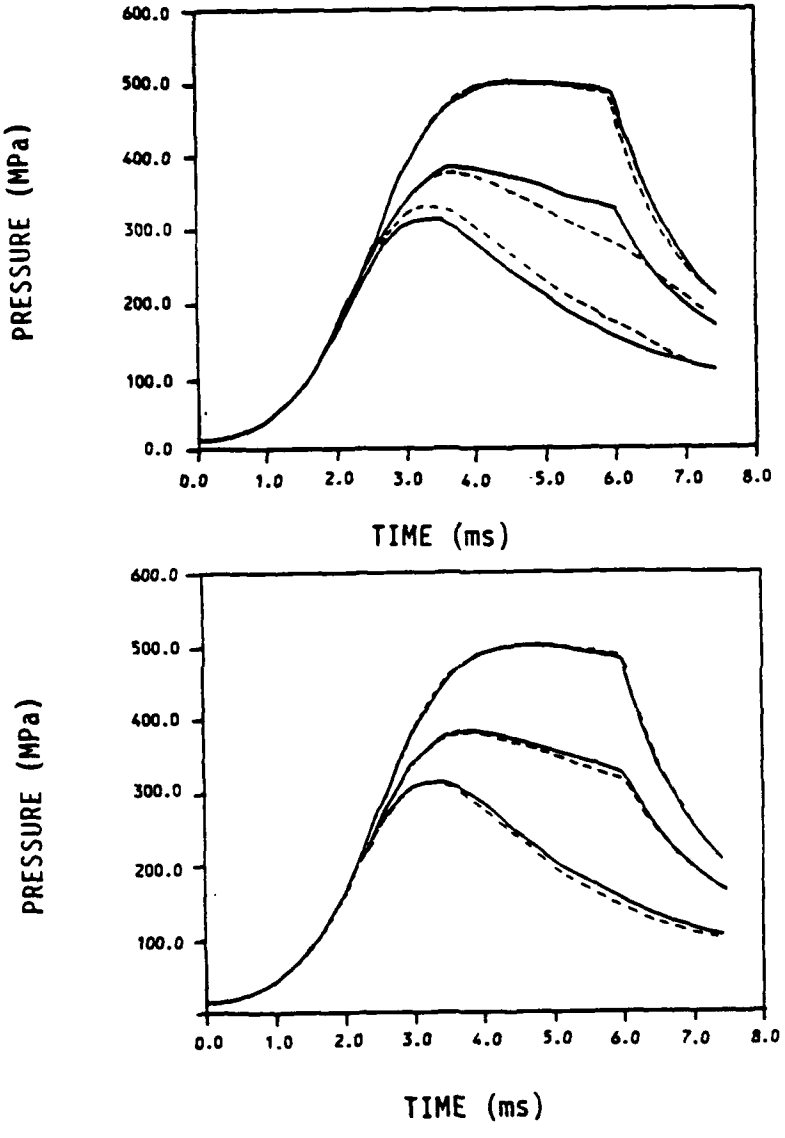

Figure 6. Comparison of Pressure vs. Time Curves for the 7 kg Projectile in the Combustion Chamber (Top Curves) at the Barrel Entrance (Middle Curves) and at the Projectile Base (Bottom Curves). The Solid Line, From a Simulation Using the Gough Model,[2] is Compared to Simulations Using the Standard Lagrange Gradient, Figure 6a (top) and the Modified Lagrange Gradient, Figure 6b (bottom).

In comparison, the modified Lagrange gradient model results show very good agreement with the one-dimensional model; see Figure 6b. The chamber and barrel entrance pressures are almost indistinguishable over the entire ballistic cycle for the two simulations. The projectile base pressures are also nearly indistinguishable over the first half of the ballistic cycle, but the modified Lagrange curve increasingly departs from the baseline curve after about 4.0 ms. This departure is below the baseline, consistent with the velocity difference noted in Table 3. This discrepancy between the modified Lagrange and one-dimensional results is attributed to the decreasing validity of both the basic Lagrange assumption, uniform gas density, as the projectile becomes farther removed from the barrel entrance, and the assumption of fixed v_{Lb} and $\dot{v}_{Lb}$ after all-burnt.

Pressure and velocity profiles in the barrel region from the simulations for the 7 kg projectile using the modified Lagrange and one-dimensional models are presented in Figures 7-11. The times for which these profiles were plotted were chosen to coincide with maximum pressure at the projectile base (3.3 ms), maximum chamber pressure (4.7 m/s), a time just after all-burnt (6.1 ms), a time when the rarefaction wave has propagated some distance down the barrel (6.5 ms), and muzzle exit (7.4 m/s).

Prior to all-burnt (3.3 ms and 4.7 ms), the modified Lagrange model produces velocity and pressure profiles which have the correct shape and are quite close to the one-dimensional profiles over the entire barrel region; see Figures 7 and 8. The departure in pressure at the projectile base, noted earlier, as well as a corresponding difference in velocity near the projectile base, has begun to appear in Figure 8.

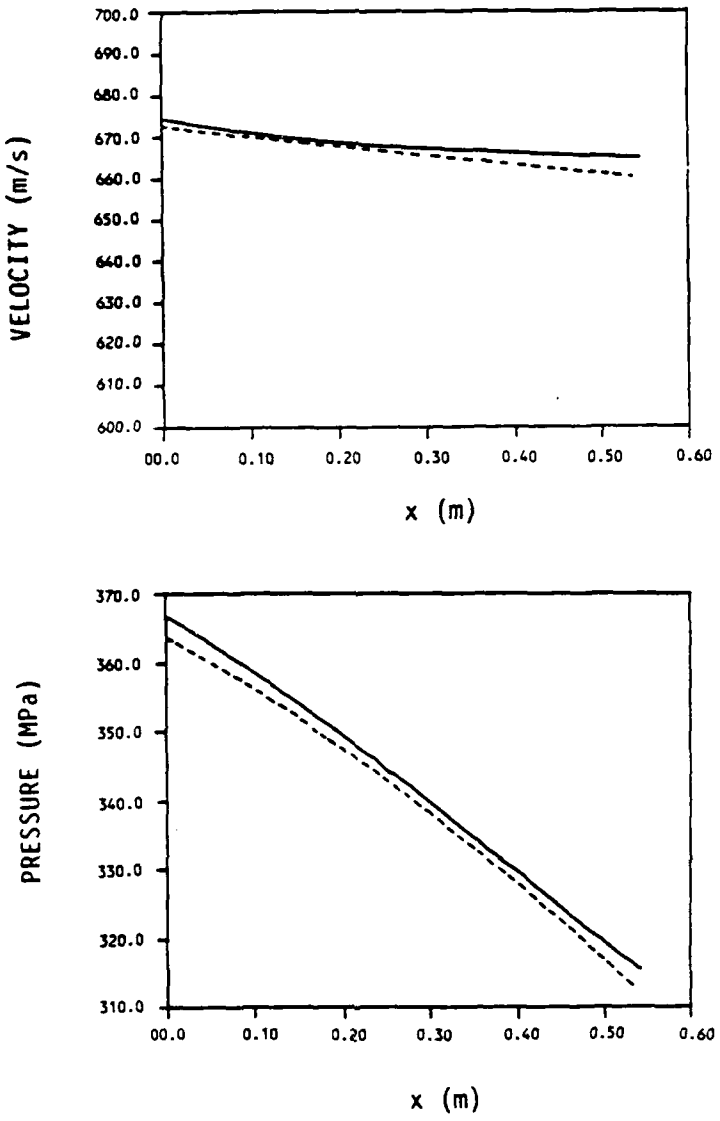

Figure 7. Comparison of Velocity and Pressure Distribution in the Barrel at t = 3.3 ms, from Simulations Using Gough Model[2] (Solid Line) and the Modified Lagrange Gradient (Dashed Line) for the 7 kg Projectile.

In Figure 9, the rarefaction wave can be seen just beginning to propagate along the barrel toward the projectile base. Again, the overall shape and magnitude of the velocity and pressure profiles are in good agreement. The differences in velocity and pressure near the projectile base have become more pronounced, about 6-7% in pressure at 6.1 ms versus about 4% at 4.7 ms.

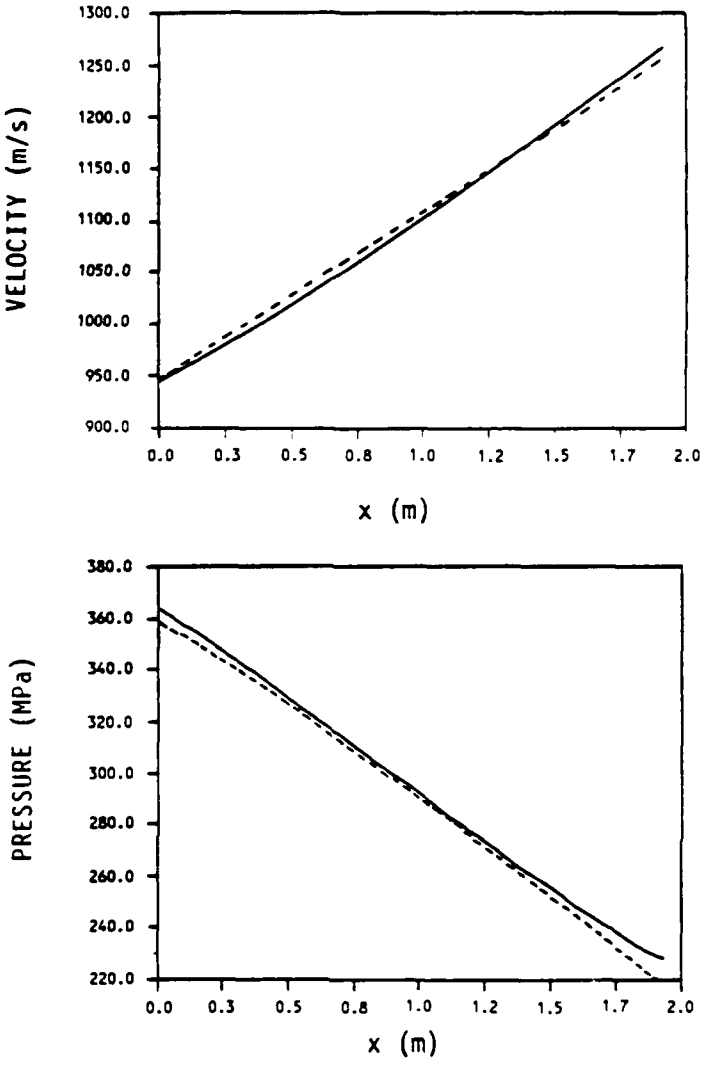

Figure 8. Comparison of Velocity and Pressure Distribution in the Barrel at t ≈ 4.7 ms, from Simulations Using Gough Model[2] (Solid Line) and the Modified Lagrange Gradient (Dashed Line) for the 7 kg Projectile.

Slightly later in time, at 6.5 ms, the rarefaction wave is well developed and has propagated about one quarter of the distance to the projectile base; see Figure 10. The velocity and pressure profiles are still in good agreement with the baseline case, and the hinge point is in approximately the correct position.

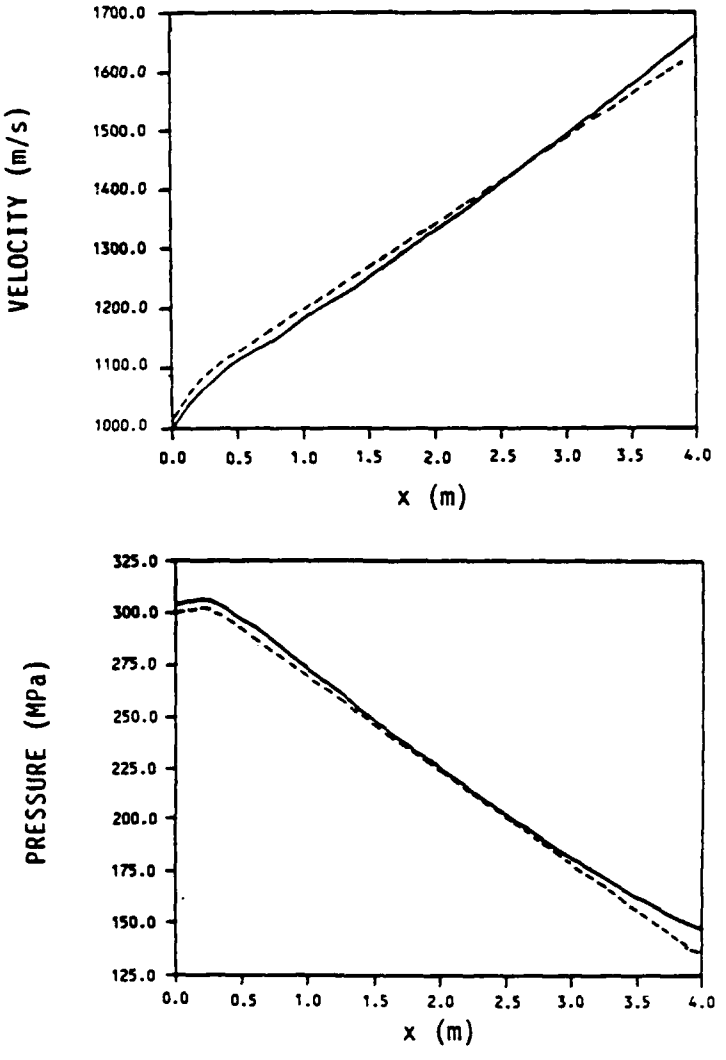

Figure 9. Comparison of Velocity and Pressure Distribution in the Barrel at t = 6.1 ms, from Simulations Using Gough Model[2] (Solid Line) and the Modified Lagrange Gradient (Dashed Line) for the 7 kg Projectile.

The pressure and velocity differences near the projectile base have continued to increase; the pressure difference at the projectile base has increased to about 8%.

At muzzle exit, Figure 11, the velocity profiles are still in very good agreement, but the modified Lagrange pressure profile has deteriorated somewhat.

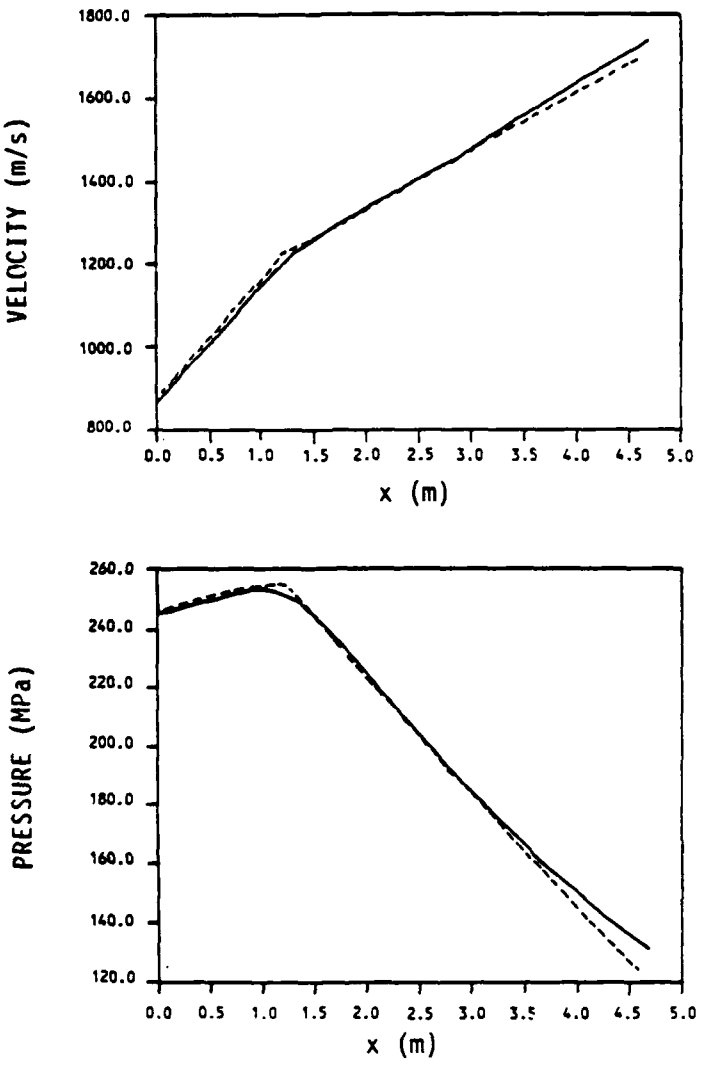

Figure 10. Comparison of Velocity and Pressure Distribution in the Barrel at t = 6.5 ms, from Simulations Using Gough Model[2] (Solid Line) and the Modified Lagrange Gradient (Dashed Line) for the 7 kg Projectile.

The shape of the pressure profile is still approximately correct; however, the departure from the baseline profile is apparent, the pressure difference at the projectile base having increased to approximately 10%. This discrepancy does not reflect the overall accuracy of the approximation, however, since the cumulative difference in projectile velocity is only about 2.5% in this case.

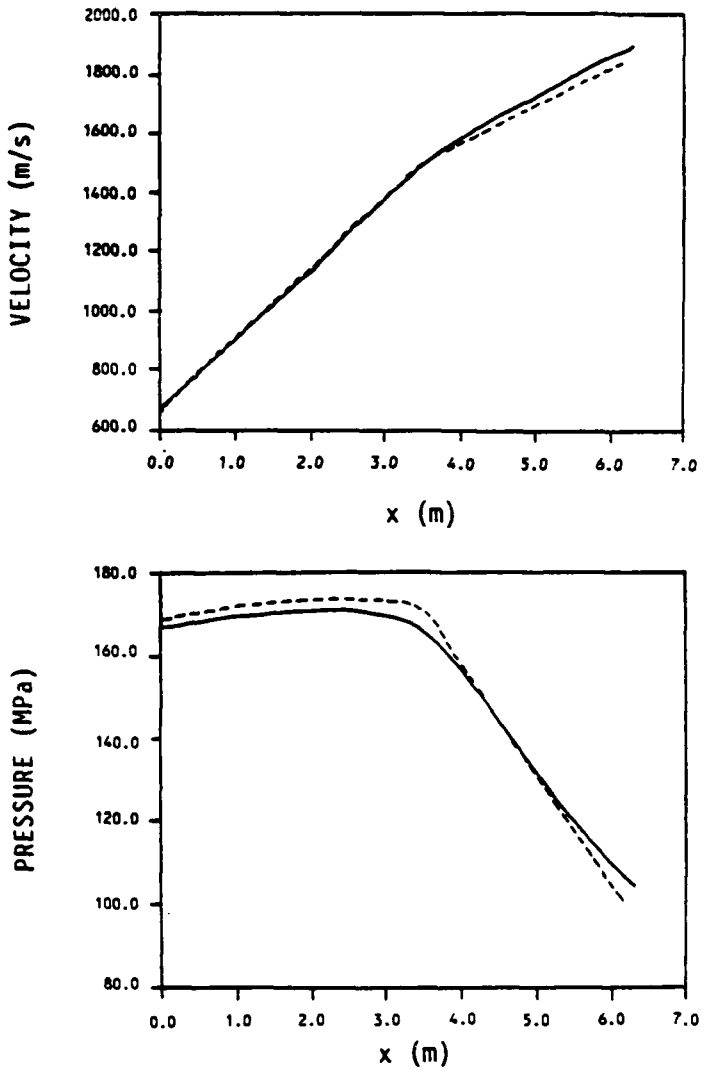

Figure 11. Comparison of Velocity and Pressure Distribution in the Barrel at t = 7.4 ms, from Simulations Using Gough Model[2] (Solid Line) and the Modified Lagrange Gradient (Dashed Line) for the 7 kg Projectile.

VIII. CONCLUSIONS

A modification of the standard Lagrange gradient model has been developed to simulate the gas flow in the barrel of a regenerative liquid propellant gun. This model accounts for the non-zero gas velocity at the entrance to the barrel,

and the existence of a rarefaction wave which travels along the barrel from the chamber toward the projectile base after all-burnt. The modified Lagrange gradient has been implemented in the lumped parameter interior ballistic model developed by Coffee, and comparisons have been made among the resulting IB model, the Coffee model with a standard Lagrange gradient, and the Gough model with a one-dimensional barrel flow model Computer simulations of a high velocity 120-mm tank cannon have been run, using these three models, for 3 projectile masses.

The modified Lagrange gradient model resulted in muzzle velocities 1.1-3.4% lower than the one-dimensional model over the velocity range 1563-2020 m/s, while the standard Lagrange model produced muzzle velocities 3.5-4.7% higher than the one-dimensional model. The pressure versus time curves obtained using the modified Lagrange gradient are in very good agreement with those from the one-dimensional model, although some discrepancy is observed at the projectile base over the latter half of the ballistic cycle. A similar comparison for the standard Lagrange gradient case shows very poor agreement with the one-dimensional model at the barrel entrance and at the projectile base over most of the ballistic cycle.

Detailed comparisons of the velocity and pressure profiles in the barrel from the modified Lagrange and one-dimensional models at five different times during the ballistic cycle have been made. These comparisons show that the profiles obtained using the modified Lagrange gradient have the correct shape and, with the exception of the pressure profile near muzzle exit, are in excellent agreement with the one-dimensional results. Overall, the modified Lagrange gradient model appears to be capable of accurately representing the physical processes in the barrel region of a regenerative liquid propellant gun and of providing an excellent overall simulation of the IB process, even in the high velocity regime.

INTENTIONALLY LEFT BLANK.

LIST OF SYMBOLS

A_B	Bore Area
a	Average Speed of Sound
C	Charge Mass
c_p	Specific Heat at Constant Pressure
h	Enthalpy
M_p	Projectile Mass
m	Mass of Gas in Barrel
P	Pressure
$\bar{P}$	Space Mean Pressure
P_{RES}	Barrel Resistance Pressure
T	Temperature
u_p	Projectile Velocity
v	Gas Velocity
x	Coordinate Along the Barrel
y	Coordinate of Projectile
γ	Ratio of Specific Heats
η	Gas Co-Volume
ρ	Gas Density
ψ	Barrel Entrance Coefficient

Subscripts:

BASE	Projectile Base
BREECH	Gun Breech
c	Combustion Chamber
H	Hinge-Point
L	Barrel Entrance
Lb	Barrel Entrance at All-Burnt
R	Projectile Base

REFERENCES

1. Coffee, T.P., "A Lumped Parameter Code for Regenerative Liquid Propellant Guns," BRL Technical Report No. BRL-TR-2703, December 1985.

2. Gough, P.S., "A Model of the Interior Ballistics of Hybrid Liquid Propellant Guns," BRL Contract Report No. BRL-CR-566, March 1987.

3. Corner, J., Theory of the Interior Ballistics of Guns, J. Wiley & Sons, Inc., New York, Copyright 1950.

4. Coffee, T.P., "The Analysis of Experimental Measurements on Liquid Regenerative Guns," BRL Technical Report No. BRL-TR-2731, May 1986.

5. Gough, P.S., BRL Contract Report in preparation.

6. Morrison, W.F., Baer, P.G., Bulman, M.J. and Mandzy, J., "The Interior Ballistics of Regenerative Liquid Propellant Guns," BRL Technical Report No. BRL-TR-2857, Oct 1987.

7. Robbins, F.W. and Horst, A.W., "Detailed Characterization of the Interior Ballistics of Slotted Stick Propellant," BRL Technical Report No. BRL-TR-2591, September 1984.

8. Mandzy, J., General Electric Company, private communication.

9. Coffee, T.P., "An Updated Lumped Parameter Code for Regenerative Liquid Propellant In-Line Guns," BRL Technical Report No. BRL-TR-2974, December 1988.

10. Gough, P.S., Contractor Report DAAK11-85-D-0002, in preparation.

11. Baer, P.G., Coffee, T.P. and Morrison, W.F., "Design Optimization for a High Performance Regenerative Liquid Propellant Gun," BRL Technical Report No. BRL-TR-2860, October 1987.

No of Copies	Organization
(Class., unlimited) 12	Administrator
(Class., limited) 2	Defense Technical Info Center
(Classified) 2	ATTN: DTIC-DDA
	Cameron Station
	Alexandria, VA 22304-6145
1	HQDA (SARD-TR)
	WASH DC 20310-0001
1	Commander
	US Army Materiel Command
	ATTN: AMCDRA-ST
	5001 Eisenhower Avenue
	Alexandria, VA 22333-0001
1	Commander
	US Army Laboratory Command
	ATTN: AMSLC-DL
	Adelphi, MD 20783-1145
2	Commander
	Armament RD&E Center
	US Army AMCCOM
	ATTN: SMCAR-MSI
	Picatinny Arsenal, NJ 07806-5000
2	Commander
	Armament RD&E Center
	US Army AMCCOM
	ATTN: SMCAR-TDC
	Picatinny Arsenal, NJ 07806-5000
1	Director
	Benet Weapons Laboratory
	Armament RD&E Center
	US Army AMCCOM
	ATTN: SMCAR-CCB-TL
	Watervliet, NY 12189-4050
1	Commander
	US Army Armament, Munitions and Chemical Command
	ATTN: SMCAR-ESP-L
	Rock Island, IL 61299-5000
1	Commander
	US Army Aviation Systems Command
	ATTN: AMSAV-DACL
	4300 Goodfellow Blvd.
	St. Louis, MO 63120-1798
1	Director
	US Army Aviation Research and Technology Activity
	Ames Research Center
	Moffett Field, CA 94035-1099

No of Copies	Organization
1	Commander
	US Army Missile Command
	ATTN: AMSMI-RD-CS-R (DOC)
	Redstone Arsenal, AL 35898-5010
1	Commander
	US Army Tank-Automotive Command
	ATTN: AMSTA-TSL (Technical Library)
	Warren, MI 48397-5000
1	Director
	US Army TRADOC Analysis Command
	ATTN: ATAA-SL
	White Sands Missile Range, NM 88002-5502
(Class. only) 1	Commandant
	US Army Infantry School
	ATTN: ATSH-CD (Security Mgr.)
	Fort Benning, GA 31905-5660
(Unclass. only) 1	Commandant
	US Army Infantry School
	ATTN: ATSH-CD-CSO-OR
	Fort Benning, GA 31905-5660
(Class. only) 1	The Rand Corporation
	P.O. Box 2138
	Santa Monica, CA 90401-2138
1	Air Force Armament Laboratory
	ATTN: AFATL/DLODL
	Eglin AFB, FL 32542-5000

Aberdeen Proving Ground

Dir, USAMSAA
ATTN: AMXSY-D
AMXSY-MP, H. Cohen

Cdr, USATECOM
ATTN: AMSTE-TO-F

Cdr, CRDEC, AMCCOM
ATTN: SMCCR-RSP-A
SMCCR-MU
SMCCR-MSI

Dir, VLAMO
ATTN: AMSLC-VL-D

No. of Copies	Organization
2	Director Defense Advanced Research Projects Agency ATTN: J. Lupo J. Richardson 1400 Wilson Boulevard Arlington, VA 22209
4	HQDA (SARD-ZT, G. Singley) (SARD-TT, I. Szkrybalo) (SARD-TC, C. Church, D. Zimmerman) WASH DC 20310
1	HQ, US Army Materiel Command ATTN: AMCICP-AD, B. Dunetz 5001 Eisenhower Avenue Alexandria, VA 22333-0001
13	Commander Armament RD&E Center US Army AMCCOM ATTN: SMCAR-TSS SMCAR-AEE-B, D. Downs SMCAR-AEE-BR, B. Brodman W. Seals A. Beardell SMCAR-AEE-W, N. Slagg SMCAR-AEE, A. Bracuti J. Lannon M. Gupta J. Salo D. Chieu SMCAR-FSS-D, L. Frauen SMCAR-FSA-S, H. Liberman Picatinny Arsenal, NJ 07806-5000
3	Commander Armament RD&E Center US Army AMCCOM ATTN: SMCAR-FSS-DA, J. Feneck R. Kopmann J. Irizarry Bldg 94 Picatinny Arsenal, NJ 07806-5000
4	Director Benet Weapons Laboratory Armament RD&E Center US Army AMCCOM ATTN: SMCAR-CCB, L. Johnson SMCAR-CCB-S, F. Heiser SMCAR-CCB-DS, E. Conroy A. Graham Watervliet, NY 12189-4050
1	Commander Materials Technology Laboratory US Army Laboratory Command ATTN: SLCMT-MCM-SB, M. Levy Watertown, MA 02172-0001
1	Commander CECOM R&D Technical Library ATTN: ASQNC-ELC-I-T, Myer Center Ft. Monmouth, NJ 07703-5000
1	Commander US Army Harry Diamond Laboratories ATTN: SLCHD-TA-L 2800 Powder Mill Road Adelphi, MD 20783-1145
1	Commander US Army Belvoir Research and Development Center ATTN: STRBE-WC, Technical Library (Vault) B-315 Fort Belvoir, VA 22060-5606
1	Commander US Army Research Office ATTN: Technical Library P.O. Box 12211 Research Triangle Park, NC 27709-2211
1	Commander Armament RD&E Center US Army AMCCOM ATTN: SMCAR-CCS-C, T. Hung Picatinny Arsenal, NJ 07806-5000

No. of Copies	Organization
2	Commandant US Army Field Artillery School ATTN: ATSF-CMW ATSF-TSM-CN, J. Spicer Fort Sill, OK 73503
1	Commandant US Army Armor Center ATTN: ATSB-CD-MLD Fort Knox, KY 40121
1	Commander Naval Surface Weapons Center ATTN: D.A. Wilson (Code G31) Dahlgren, VA 22448-5000
1	Commander Naval Surface Weapons Center ATTN: J. East (Code G33) Dahlgren, VA 22448-5000
2	Commander US Naval Surface Weapons Center ATTN: O. Dengel K. Thorsted Silver Spring, MD 20902-5000
1	Commander (Code 3247) Naval Weapons Center Gun Systems Branch China Lake, CA 93555-6000
1	Superintendent Naval Postgraduate School Department of Mechanical Engineering ATTN: Code 1424, Library Monterey, CA 93943
1	AFOSR/NA (L. Caveny) Building 410 Bolling AFB Washington, DC 20332
1	Commandant USAFAS ATTN: ATSF-TSM-CN Fort Sill, OK 73503-5600
1	Director Jet Propulsion Laboratory ATTN: Technical Library 4800 Oak Grove Drive Pasadena, CA 91109

No. of Copies	Organization
2	Director National Aeronautics and Space Administration ATTN: MS-603, Technical Library MS-86, Dr. Povinelli 21000 Brookpark Road Lewis Research Center Cleveland, OH 44135
1	Director National Aeronautics and Space Administration Manned Spacecraft Center Houston, TX 77058
10	Central Intelligence Agency Office of Central Reference Dissemination Branch Room GE-47 HQS Washington, DC 20502
1	Central Intelligence Agency ATTN: Joseph E. Backofen HQ Room 5F22 Washington, DC 20505
1	Calspan Corporation ATTN: Technical Library P.O. Box 400 Buffalo, NY 14225
8	General Electric Ordnance System Division ATTN: J. Mandzy, OP43-220 R.E. Mayer H. West W. Pasko R. Pate I. Magoon J. Scudiere Minh Luu 100 Plastics Avenue Pittsfield, MA 01201-3698
1	General Electric Company Armament Systems Department ATTN: D. Maher Burlington, VT 05401
1	Honeywell, Inc. ATTN: R.E. Tompkins MN38-3300 10400 Yellow Circle Drive Minnetonka, MN 55343

No. of Copies	Organization
1	IITRI ATTN: Library 10 West 35th Street Chicago, IL 60616
1	Olin Chemicals Research ATTN: David Gavin P.O. Box 586 Chesire, CT 06410-0586
1	Paul Gough Associates ATTN: Paul Gough 1048 South Street Portsmouth, NH 03801-5423
1	Safety Consulting Engineer ATTN: Mr. C. James Dahn 5240 Pearl Street Rosemont, IL 60018
1	Sandia National Laboratories ATTN: R. Rychnovsky, Div 8152 P.O. Box 969 Livermore, CA 94551-0969
1	Sandia National Laboratories ATTN: S. Griffiths, Div 8244 P.O. Box 969 Livermore, CA 94551-0969
1	Sandia National Laboratories ATTN: R. Carling, Div 8152 P.O. Box 969 Livermore, CA 94551-0969
1	Science Applications, Inc. ATTN: R. Edelman 23146 Cumorah Crest Woodland Hills, CA 91364
2	Science Applications International Corporation ATTN: Dr. F.T. Phillips Dr. Fred Su 10210 Campus Point Drive San Diego, CA 92121

No. of Copies	Organization
1	Science Applications International Corporation ATTN: Norman Banks 4900 Waters Edge Drive Suite 255 Raleigh, NC 27606
1	Sundstrand Aviation Operations ATTN: Mr. Owen Briles P.O. Box 7202 Rockford, IL 61125
1	Veritay Technology, Inc. ATTN: E.B. Fisher 4845 Millersport Highway P.O. Box 305 East Amherst, NY 14051-0305
1	Director The Johns Hopkins University Applied Physics Laboratory Johns Hopkins Road Laurel, MD 20707
2	Director CPIA The Johns Hopkins University ATTN: T. Christian Technical Library Johns Hopkins Road Laurel, MD 20707
1	University of Illinois at Chicago ATTN: Professor Sohail Murad Department of Chemical Engineering Box 4348 Chicago, IL 60680
1	University of Maryland at College Park ATTN: Professor Franz Kasler Department of Chemistry College Park, MD 20742
1	University of Missouri at Columbia ATTN: Professor R. Thompson Department of Chemistry Columbia, MO 65211
1	University of Michigan ATTN: Professor Gerard M. Faeth Department of Aerospace Engineering Ann Arbor, MI 48109-3796

No. of Copies	Organization
1	University of Missouri at Columbia ATTN: Professor F.K. Ross Research Reactor Columbia, MO 65211
1	University of Missouri at Kansas City Department of Physics ATTN: Professor R.D. Murphy 1110 East 48th Street Kansas City, MO 64110-2499
1	Pennsylvania State University Department of Mechanical Engineering ATTN: Professor K. Kuo University Park, PA 16802
2	Princeton Combustion Research Laboratories, Inc. ATTN: N.A. Messina M. Summerfield 4275 US Highway One North Monmouth Junction, NJ 08852
1	University of Arkansas Department of Chemical Engineering ATTN: J. Havens 227 Engineering Building Fayetteville, AR 72701
3	University of Delaware Department of Chemistry ATTN: Mr. James Cronin Professor Thomas Brill Mr. Peter Spohn Newark, DE 19711
1	University of Texas at Austin Bureau of Engineering Research ATTN: BRC EME133, Room 1.100 H. Fair 10100 Burnet Road Austin, TX 78758

No. of Copies	Organization
1	Dr. Clive Woodley GS2 Division Building R31 RARDE Fort Halstead Sevenoaks, Kent TN14 7BT England

USER EVALUATION SHEET/CHANGE OF ADDRESS

This Laboratory undertakes a continuing effort to improve the quality of the reports it publishes. Your comments/answers to the items/questions below will aid us in our efforts.

1. BRL Report Number BRL-TR-3073 Date of Report JANUARY 1990

2. Date Report Received _____

3. Does this report satisfy a need? (Comment on purpose, related project, or other area of interest for which the report will be used.) _____

4. How specifically, is the report being used? (Information source, design data, procedure, source of ideas, etc.) _____

5. Has the information in this report led to any quantitative savings as far as man-hours or dollars saved, operating costs avoided or efficiencies achieved, etc? If so, please elaborate. _____

6. *General Comments*. What do you think should be changed to improve future reports? (Indicate changes to organization, technical content, format, etc.)

CURRENT ADDRESS

Name

Organization

Address

City, State, Zip

7. If indicating a Change of Address or Address Correction, please provide the New or Correct Address in Block 6 above and the Old or Incorrect address below.

OLD ADDRESS

Name

Organization

Address

City, State, Zip

(Remove this sheet, fold as indicated, staple or tape closed, and mail.)